



# Improving the Electrochemical Performance and Structural Stability of LiNi0.8Co0.15Al0.05O2 Cathode Material at High Voltage Charging through Ti Substitution

Q. Qiu, Z. Shadike

To be published in "ACS Applied Materials & Interfaces"

June 2019

## **Chemistry Department**

### **Brookhaven National Laboratory**

## **U.S. Department of Energy**

USDOE Office of Energy Efficiency and Renewable Energy (EERE), Vehicle Technologies Office (EE-3V)

Notice: This manuscript has been authored by employees of Brookhaven Science Associates, LLC under Contract No. DE-SC0012704 with the U.S. Department of Energy. The publisher by accepting the manuscript for publication acknowledges that the United States Government retains a non-exclusive, paid-up, irrevocable, world-wide license to publish or reproduce the published form of this manuscript, or allow others to do so, for United States Government purposes.

#### **DISCLAIMER**

This report was prepared as an account of work sponsored by an agency of the United States Government. Neither the United States Government nor any agency thereof, nor any of their employees, nor any of their contractors, subcontractors, or their employees, makes any warranty, express or implied, or assumes any legal liability or responsibility for the accuracy, completeness, or any third party's use or the results of such use of any information, apparatus, product, or process disclosed, or represents that its use would not infringe privately owned rights. Reference herein to any specific commercial product, process, or service by trade name, trademark, manufacturer, or otherwise, does not necessarily constitute or imply its endorsement, recommendation, or favoring by the United States Government or any agency thereof or its contractors or subcontractors. The views and opinions of authors expressed herein do not necessarily state or reflect those of the United States Government or any agency thereof.

# Improving the Electrochemical Performance and

# Structural Stability of LiNi<sub>0.8</sub>Co<sub>0.15</sub>Al<sub>0.05</sub>O<sub>2</sub>

# Cathode Material at High Voltage Charging

## through Ti Substitution

Qi-Qi Qiu,<sup>a</sup> Zulipiya Shadike,<sup>b</sup> Qin-Chao Wang,<sup>a</sup> Xin-Yang Yue,<sup>a</sup> Xun-Lu Li,<sup>a</sup> Shan-Shan Yuan,<sup>a</sup> Fang Fang,<sup>a</sup> Xiao-Jing Wu,<sup>a</sup> Adrian Hunt,<sup>c</sup> Iradwikanari Waluyo,<sup>c</sup> Seong-Min Bak,<sup>b\*</sup> Xiao-Qing Yang,<sup>b\*</sup> Yong-Ning Zhou<sup>a\*</sup>

- a. Department of Materials Science, Fudan University, Shanghai 200433, China.
- b. Chemistry Division, Brookhaven National Laboratory (BNL), Upton, New York 11973, USA.
- c. National Synchrotron Light Sources II (NSLS-II), Brookhaven National Laboratory, Upton, New York, 11973, USA

**KEYWORDS:** high voltage charging, structural stability, Ti substitution, layered cathode, lithium-ion battery.

ABSTRACT: LiNi<sub>0.8</sub>Co<sub>0.15</sub>Al<sub>0.05</sub>O<sub>2</sub> (NCA) has been proven to be a good cathode material for lithium-ion batteries (LIBs), especially in electric vehicle applications. However, further elevating energy density of NCA is very challenging. To increase the charging voltage of NCA is an effective method, but its structural instability remains a problem. In this work, we revealed that titanium substitution could improve cycle stability of NCA under high cut-off voltage significantly. Titanium ions with a relatively larger ion radius could modify the oxygen lattice and change the local coordination environment of NCA, leading to decreased cation migration, better kinetic and thermodynamic properties, and improved structural stability. As a result, Ti-substituted NCA cathode exhibits impressive reversible capacity (198 mA h g<sup>-1</sup> at 0.1 C) with considerable cycle stability under a cut-off voltage up to 4.7 V. It is also revealed that Ti could suppress oxygen release in high voltage region, benefitting to cycle and thermal stability. This work provides valuable insight into the design of high voltage layered cathode materials for high-energy-density LIBs.

#### 1. INTRODUCTION

Lithium-ion batteries (LIBs) have been successfully used as portable power sources for commercial electronic devices in the past 30 years.<sup>1</sup> However, as the first commercialized and dominant cathode material for LIBs, LiCoO<sub>2</sub> is hard to meet the ever-increasing demand for electric vehicle applications owing to high cost and limited resource of Co.<sup>2</sup> In this regard, alternative cathode materials for LIBs have been extensively studied to meet the requirements of

high energy density and low cost. Among them, LiNi<sub>0.8</sub>Co<sub>0.15</sub>Al<sub>0.05</sub>O<sub>2</sub> (NCA) was developed to be one of the most favorable candidates as a cathode material for LIBs.<sup>3-5</sup> Via partial substitution of nickel with cobalt and aluminum, NCA shows improved cycle stability while maintaining the high capacity of LiNiO<sub>2</sub>. 6,7 In the practical application of NCA cathode, a relatively low cut-off voltage (~4.2 V) has to be set for NCA batteries during cycling in order to keep its structural stability. Although increasing the cut-off voltage is considered to be the easiest way to increase capacity and energy density for layer-structured cathode, severe capacity fading and structural deterioration caused by charging voltage over 4.2 V have been the major concern for utilizing this effective approach.<sup>8,9</sup> Further improvement of the energy density and safety of NCA is hindered by the following issues: (1) The formation of electrochemical inactive rock-salt phase. An inactive rocksalt structured NiO phase is formed on the surface of NCA and thickened during cycling. 9,10 It has been demonstrated that the increased cut-off voltage will aggravate Ni migration from transitionmetal layer to lithium layer and cause side reaction between electrode and electrolyte, accelerating transformation into inactive rock-salt phase and deterioration of dynamical performance. (2) The release of oxygen: During high-voltage operation, when Ni and Co are oxidized to high valence, the oxygen ions can be oxidized and cause O<sub>2</sub> gas release and irreversible structural changes. 9,12,13 (3) Microcracks: Intergranular cracks and intragranular cracks can be formed and propagated rapidly at high cut-off voltages induced by the excessive lattice expansion and shrinkage, which further exacerbates the mechanical failure of the crystal structure. 14-16

It has been widely reported that surface modification (Al<sub>2</sub>O<sub>3</sub>,<sup>17</sup> ZnO,<sup>18</sup> Co<sub>3</sub>O<sub>4</sub>,<sup>19</sup> LiFePO<sub>4</sub>,<sup>20</sup> Li<sub>2</sub>TiO<sub>3</sub>,<sup>21</sup> Li<sub>4</sub>Mn<sub>5</sub>O<sub>12</sub><sup>22</sup>) and ion substitution (Ti<sup>4+</sup>,<sup>23-25</sup> Mg<sup>2+</sup>,<sup>26</sup> Zr<sup>4+</sup>,<sup>27</sup> Br<sup>-</sup>,<sup>28</sup> F<sup>-</sup><sup>29</sup>) are effective methods for improving electrochemical performance of layered cathode materials. Among them, titanium substitution is found to be effective in stabilizing structure and improving cycle

performance of layer-structured cathodes. Density functional theory (DFT) calculations revealed that a small amount of Ti substitution (<5%) in LiNi<sub>x</sub>Mn<sub>x</sub>Co<sub>1-2x</sub>O<sub>2</sub> could reduce the changes of lithium interstitial volume and structural distortion during cycling.<sup>23</sup> 2% molar concentration of Ti substitution is confirmed to be able to reduce the formation of NiO inactive phase in LiNi<sub>0.8</sub>Co<sub>0.1</sub>Mn<sub>0.1</sub>O<sub>2</sub>, and to improve cycle performance between 2.8 and 4.5 V.<sup>24,25</sup> However, the detailed effects of Ti substitution in NCA on structural evolution and electrochemical performance, especially at high voltage cycling above 4.5 V has not been thoroughly studied and well understood.

In this paper, we demonstrate that the appropriate amount of Ti substitution could enable NCA cathode to be operated with a high cut-off voltage of 4.7 V, with promising cycle stability and rate capability. The origin of the effects of Ti substitution on the surface composition, kinetic and thermodynamic characteristics of NCA cathode as well as on the crystal structure evolution during high-voltage charging was systematically studied.

#### 2. EXPERIMENTAL

**2.1. Material preparation.** The hydroxide precursor  $Ni_{0.8}Co_{0.15}Al_{0.05}(OH)_2$  was synthesized by a co-precipitation method. As starting materials,  $NiSO_4 \cdot 6H_2O$ ,  $CoSO_4 \cdot 7H_2O$  and  $Al_2(SO_4)_3 \cdot 18H_2O$  were dissolved in distilled water with a molar ratio of Ni: Co: Al = 80: 15: 5 with a concentration of 1 M. The solution was pumped slowly into a continuous stirred reactor (1L), with a 2 M NaOH solution and a 2 M NH<sub>4</sub>·OH solution fed into the reactor simultaneously. The pH value is kept at 10.5. The reaction temperature, feeding speed, as well as stirring speed were well controlled in the system. After being filtered and washed with distilled water thoroughly, the pale green precipitates were dried at 100 °C for 12 h. The pristine LiNi<sub>0.8</sub>Co<sub>0.15</sub>Al<sub>0.05</sub>O<sub>2</sub> (NCA) was prepared by mixing

the precursor with 5% excess LiOH·H<sub>2</sub>O in an agate mortar. Afterwards, the mixture was sintered at 550 °C for 5 h, then 750 °C for 15 h in sequence in oxygen atmosphere. The Ti-doped samples were prepared by mixing TiO<sub>2</sub> with the precursor and LiOH·H<sub>2</sub>O in a molar ratio of Li: Ti = 1:0.005 (NCAT-0.5), 1:0.01 (NCAT-1) and 1:0.02 (NCAT-2) followed by the same calcining process described above.

- **2.2. Material characterization.** Crystal structure and structural evolution during cycling of the as-prepared samples were detected by X-ray diffraction (XRD, Bruker,  $\lambda = 0.154$  nm) covering two theta angles from 10° to 80°. The Li<sup>+</sup>/Ni<sup>2+</sup> cation mixing and lattice parameters were obtained from XRD refinement applied by Rietveld method using GSAS+EXPGUL<sup>30</sup> The micromorphology of precursor and cathode materials were observed by scanning electron microscopy (SEM, Cambridge S-360). The intuitionistic surface crystal structure and energy-dispersive X-ray spectroscopy (EDS) of the samples were collected using field-emission transmission electron microscopy (FETEM). The thermal stability was measured using differential scanning calorimetry (DSC). X-ray absorption spectroscopy (XAS) was measured at QAS (7-BM) of National Synchrotron Light Source-II (NSLS-II) and BL14W1 of Shanghai Synchrotron Radiation Facility (SSRF). O K-edge XAS were measured using partial fluorescence yield (PFY) mode and total electron yield (TEY) mode at IOS (23-ID-2) of NSLS-II. XAS data were processed with Athena.<sup>31</sup>
- **2.3. Electrochemistry.** The cathode slurry consisting of 70 wt.% active materials, 20 wt.% carbon black and 10 wt.% polyvinylidene fluoride (PVDF) was homogeneously mixed and dispersed in N-methyl-2-pyrrolidone (NMP). The slurry was coated onto aluminium foil and dried at 70 °C. The electrodes were prepared by punching the dried laminate into round disks (diameter: 12 mm).

Coin cells (CR2032) were assembled in an argon-filled glovebox (OMNI-LAB, VAC) using 1 M LiPF<sub>6</sub> in a solution of ethylene carbonate/diethyl carbonate (1:1 in volume) as electrolyte.

Galvanostatic charge-discharge and rate performance were performed on a Land CT2001A system. The current density and capacity were calculated using the mass of active materials on each electrode disk. The cyclic voltammetry (CV) measurements were carried out on an electrochemical workstation (SP-300, Bio-Logic).

#### 3. RESULTS AND DISCUSSION

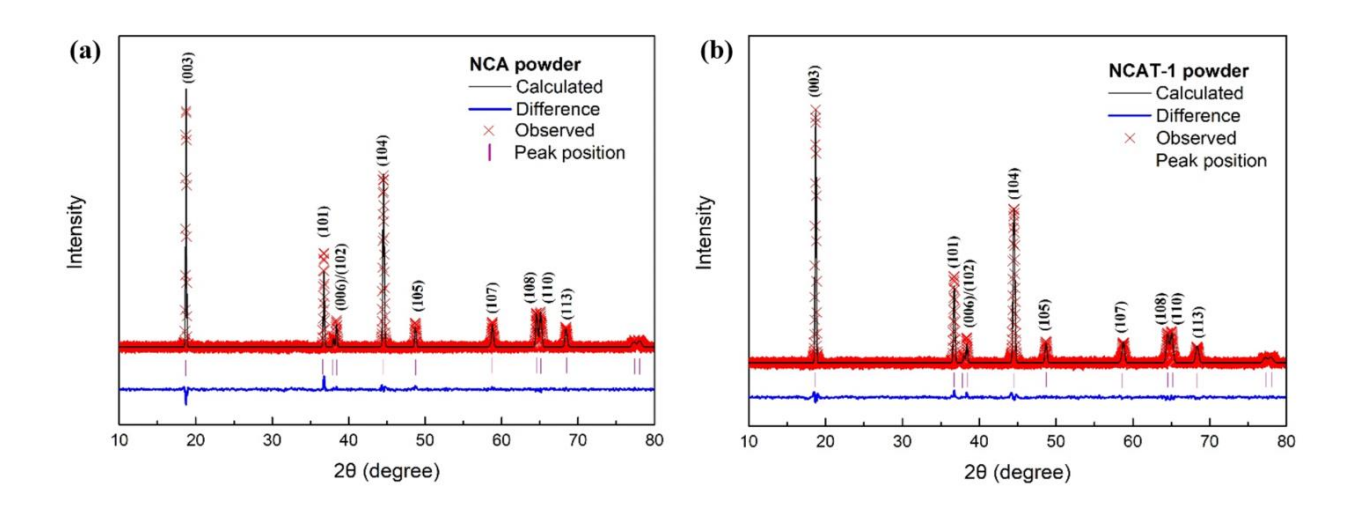


**Figure 1.** Rietveld refinement results of XRD patterns of (a) NCA and (b) NCAT-1.

**3.1. Crystal structure.** Figure 1 presents the XRD patterns and Rietveld refinement results of the pristine NCA and Ti-doped NCAT-1 (XRD patterns of NCAT-0.5 and NCAT-2 are presented in Figure S1). Both patterns exhibit sharp diffraction peaks, suggesting the as-prepared materials are well crystallized. All peaks can be assigned to  $\alpha$ -NaFeO<sub>2</sub> hexagonal phase (space group: R-3m) with Li ion, transition metal ions and oxygen ion at the 3a, 3b, and 6c sites respectively.<sup>32</sup> No

impurity phase is observed and both of the (003) and (104) crystal plane diffraction peaks slightly shift to lower angle indicating the enlargement of cell parameters with increasing of Ti doping content. For a more visual representation, the structure parameters are derived from Rietveld refinements and listed in Table 1. The lattice parameters are increased for both of a (from 2.8646(1) Å to 2.8677(1) Å) and c (from 14.1916(4) Å to 14.2141(2) Å) with increasing Ti content (from 0.5% to 2%), attributed to the larger radius of Ti<sup>4+</sup> (0.605 Å) comparing with the transition metal ions (Ni<sup>3+</sup>: 0.560 Å, Co<sup>3+</sup>: 0.545 Å, Al<sup>3+</sup>: 0.535 Å).

From Table 1, it is found that Ti doping enlarges the ratio of c/a and unit cell volume, which is beneficial to the transportation of lithium-ion, giving better kinetic properties and rate performance.<sup>33</sup> Since Ni<sup>2+</sup> can hardly be oxidized completely to Ni<sup>3+</sup> during the synthesis process, a small amount of residual Ni<sup>2+</sup> can be found in lithium layer, namely, cation mixing owing to the similar radii of Li<sup>+</sup> (0.76 Å) and Ni<sup>2+</sup>(0.69 Å) ions.<sup>34</sup> Since titanium is an early transition metal, the d orbital of titanium is more delocalized than that of later transition metals like Ni and Co. Substitution of Ti<sup>4+</sup> can strengthen the metal-metal interaction in the transition-metal layers which restrains the cross-layer migration of Ni<sup>2+</sup> and further reduces the cation mixing. Although the introduction of Ti<sup>4+</sup> in NCA could increases the content of Ni<sup>2+</sup> to some extent for charge compensation, the effect of little increase of Ni<sup>2+</sup> is negligible compared with the effect of inhibiting transition metal migration due to the changing of local electron configuration environment in the situation of trace Ti doping ( $\leq 2\%$ ). The  $I_{003}/I_{104}$  value has been considered an important indicator of cation mixing. Comparing the XRD patterns in Figure 1 and S1, the I<sub>003</sub>/I<sub>104</sub> value increases evidently after Ti doping, suggesting the reduction of cation mixing. The exact values of cation mixing obtained from XRD refinement are presented in Table 1. NCAT-1 shows the lowest cation mixing which is supposed to have better electrochemical performance. Similar

to Li[Ni<sub>0.5</sub>Mn<sub>0.5-x</sub>Ti<sub>x</sub>]O<sub>2</sub> layered cathode,<sup>35</sup> moderate Ti substitution is confirmed to be an effective approach to suppress cation mixing in NCA while maintaining the integrity of the layered structure.

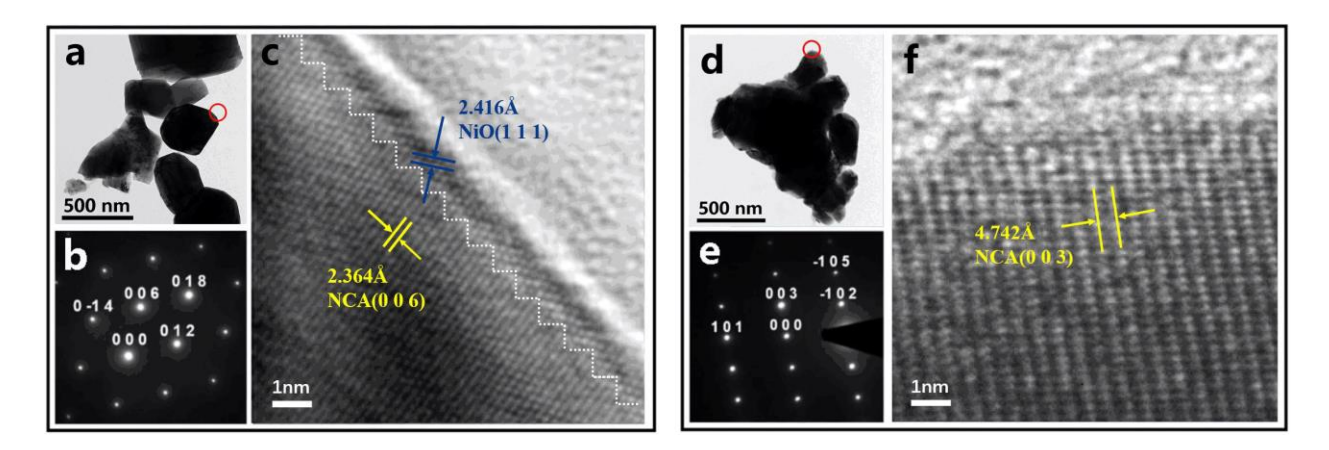


**Figure 2.** (a) Low-magnification TEM image, (b) SAED pattern and (c) HRTEM image of NCA. (d) Low-magnification TEM image, (e) SAED pattern and (f) HRTEM image of NCAT -1.

To clarify the influence of Ti doping on the surface morphology and internal structure of NCA, transmission electron microscopy (TEM) with selected-area electron diffraction (SAED) were used to investigate the NCA and NCAT-1 samples. Typical low-magnification bright-field TEM images of the two samples are exhibited in Figure 2a and d, respectively. The pristine particle sizes of both samples are about several hundreds of nanometers, which agrees well with SEM observations shown in Figure S2. The composition of the synthesized samples is congruent with the expectation and Ti is indeed introduced into the lattice according to the EDS analysis of NCA and NCAT-1 samples (Figure S3). Figure 2b and e show hexagonal symmetry spots in the corresponding SAED patterns of the two samples, suggesting the single crystalline feature of the two samples. Figure 2c and f present the high resolution TEM (HRTEM) images captured from the red circle regions marked in Figure 2a and d, respectively. A zigzag phase boundary can be clearly observed in Figure 2c between two different types of lattices with the interplanar distances

of 2.364 Å and 2.416 Å, which are attributed to (006) plane of the layered hexagonal phase of NCA and (111) plane of the rock-salt phase of NiO, respectively. In contrast, there is only one set of lattice fringes with an interplanar distance of 4.742 Å (Figure 2f), attributed to (003) plane of the layered hexagonal phase found in NCAT-1 sample. The reduce of surface NiO layer confirms that the doping of Ti<sup>4+</sup> can significantly suppress the formation of the high resistance and electrochemical inactive rock-salt NiO phase. As mentioned above, titanium ions with more delocalized d orbitals can strengthen the metal-oxygen bonding of the M-O<sub>6</sub> octahedral and metal-metal interaction in transition metal layers, thus suppressing the migration of transition metal ions. It is known that the rock-salt NiO phase on the NCA surface is formed due to Ni migration and oxygen release on the surface. Therefore, Ti doping can stabilize layered structure and suppress NiO phase formation.

**3.2. Electrochemical performance.** The cycle performance of the as-synthesized samples at 0.1 C (20 mA g<sup>-1</sup>) rate between 3.0 and 4.7 V is plotted in Figure 3a. The pristine NCA sample displays an initial discharge capacity of 178.2 mA h g<sup>-1</sup> and undergoes a rapid decay with only 45.5% capacity remaining after 100 cycles. The performance degradation is mainly resulted from the structure collapse of the cathode and surface passivation during the high voltage charge. In contrast, the Ti-doped samples show enhanced cycle stability with capacity retention improved to over 80% after 100 cycles. NCAT-1 sample with the lowest cation mixing delivers the best capacity retention of 86.9% with the highest reversible capacity of about 180 mA h g<sup>-1</sup>. The initial charge/discharge profiles and coulombic efficiency of the four samples are shown in Figure S4. With the increase of Ti doping amount from 0 to 1%, the initial discharge capacity increases along with the increase of coulombic efficiency, which is consistent with the reduced cation mixing confirmed by XRD

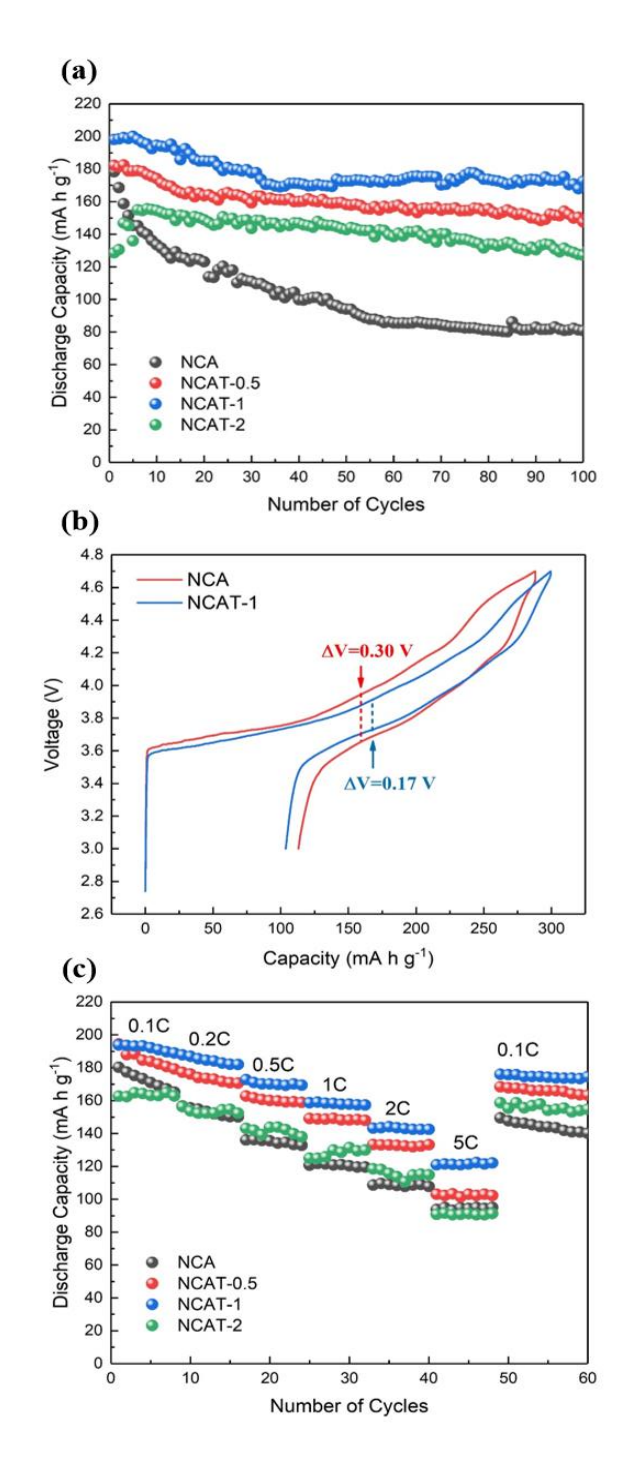


**Figure 3.** (a) Cycle performance of NCA, NCAT-0.5, NCAT-1 and NCAT-2 samples at 0.1 C (20 mA g<sup>-1</sup>) between 3.0 and 4.7 V at room temperature. (b) The initial charge/discharge profiles of NCA and NCAT-1 samples. (c) Rate performance with current rates from 0.1 C to 5 C at room temperature.

refinements. However, when the Ti doping amount increases to 2%, the capacity suffers noticeable losses with a little decrease of coulombic efficiency. It is probably resulted from the formation of impurity phase due to the excess amount of Ti. 36 These results suggest that moderate amount of Ti doping can improve the initial coulombic efficiency of NCA during high voltage cycling by stabilizing the crystal structure. Figure 3b shows the initial charge/discharge curves of NCA and NCAT-1. The voltage difference between the charge and discharge plateaus decreases from 0.30 to 0.17 V after Ti doping. The charge/discharge curves of the two samples in the 10<sup>th</sup> and 50<sup>th</sup> cycles are shown in Figure S5. It can be observed that the voltage difference between the charge and discharge plateaus of NCAT-1 sample is much lower than NCA sample after cycling. It confirms that titanium doping can improve the kinetics property of NCA cathode effectively.

The rate capabilities of the four samples from 0.1 C to 5 C in the voltage range of 3.0 - 4.7 V are displayed in Figure 3c. NCAT-1 has the best performance with stable reversible capacities of 198, 189, 174, 162, 147 and 125 mA h g<sup>-1</sup> at 0.1, 0.2, 0.5, 1, 2 and 5 C, respectively, higher than the other samples. When the current density was set back to 0.1 C, an impressive discharge capacity of 180 mA h g<sup>-1</sup> was recovered. In contrast, NCA has only 95 mA h g<sup>-1</sup> at 5 C and 149 mA h g<sup>-1</sup> can be recovered at 0.1C. The improvement on rate capability could be credited to the Tisubstitution induced expansion of Li<sup>+</sup> conduction channel (Table 1) and the suppression of high impedance rock-salt NiO phase formation. For comparison, the cycle performance of pristine and Ti doped NCA cathodes at 1 C rate under a normal cut-off voltage of 4.3 V is shown in Figure S6. The Ti-doped samples show better cycle stability than the pristine one between 3.0 and 4.3 V, except NCAT-2. It indicates that small amount of Ti doping is also effective to improve cycle performance of NCA in the normal voltage range. However, the reversible capacity is much lower than the cells tested between 3.0 and 4.7 V.

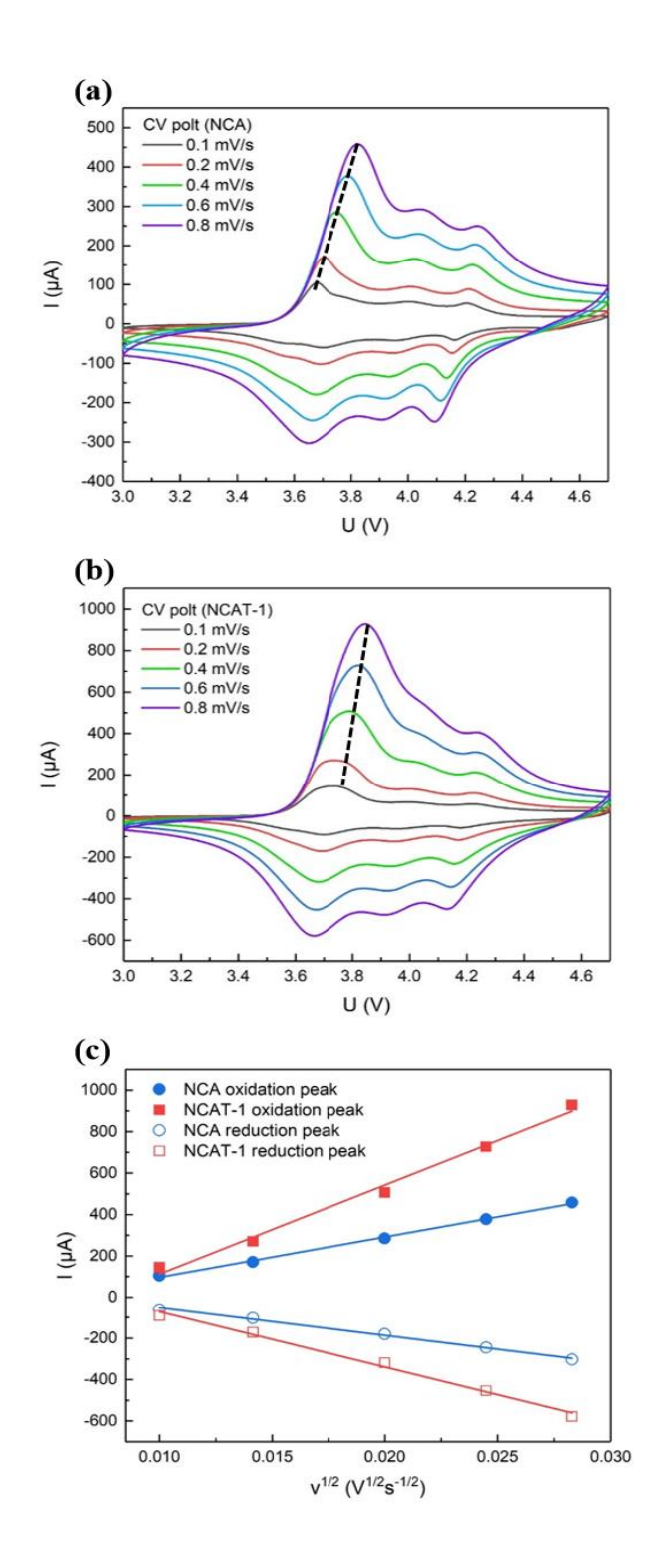


**Figure 4.** (a) Cyclic voltammogram of NCA at scanning rates from 0.1 to 0.8 mV s<sup>-1</sup>. (b) Cyclic voltammogram of NCAT-1 at scanning rates from 0.1 to 0.8 mV s<sup>-1</sup>. (c) Plots of peak current as a function of the square root of scan rate  $(v^{1/2})$ .

**3.3. Kinetic properties.** To study the effects of reduced cell polarization and enhanced rate capability of Ti-substituted NCA, the kinetic property expressed as Li-ion diffusion process in NCA and NCAT-1 electrodes was further studied by testing the cyclic voltammetry (CV) at different scan rates. The shift of peak position and evolution of peak current are associated with the kinetics of Li insertion/extraction in layer structure. Figure 4a and b show the CV profiles of NCA and NCAT-1 electrodes with scan rates increasing from 0.1 to 0.8 mV s<sup>-1</sup> between 3.0-4.7 V, respectively. In general, with scan rate increasing, the interval of corresponding oxidation and reduction peaks expands accompanied with increased peak currents  $(I_p)$ . The peak position shift of NCAT-1 is less than that of NCA as shown in Figure 4a and b. On the other hand, the  $I_p$  of NCAT-1 sample is larger than that of NCA sample. Both of these indicate a better kinetic characteristic for the NCAT-1 sample with titanium doping. It is known that the diffusion coefficient of Li<sup>+</sup> is approximately proportional to the ratio of the peak current  $(I_p)$  to square root of scan rate  $(v^{1/2})$ .  $^{30, 37}$  As shown in Figure 4c,  $I_p$  exhibits a good linear dependence on  $v^{1/2}$  both for intercalation and deintercalation process. The slope of the profile for NCAT-1 is obviously higher than that of NCA, suggesting that Li<sup>+</sup> diffusion in the NCA lattice is significantly improved by Ti-substitution.

**3.4. Structural stability during cycling.** XRD was performed to monitor the structure evolution of NCA and NCAT-1 during the first charge, further elucidating the intrinsic cause of the different cycle performance from the aspect of crystal structure. An elevated cut-off voltage of 5.0 V was set to observe complete structure evolution upon charging. A series of XRD patterns of the two samples were collected at various charge states from 3.6 V to 5.0 V at 0.1 C (Figure 5a,b). In order to eliminate the interference of angular deviation, all XRD patterns were calibrated by the (220) diffraction peak of aluminum foil. Similar to the structure evolution of LiNi<sub>0.8</sub>Co<sub>0.15</sub>Al<sub>0.05</sub>O<sub>2</sub> reported in literature, <sup>38</sup> the (003) diffraction peaks of both NCA and NCAT-1 first shift to lower

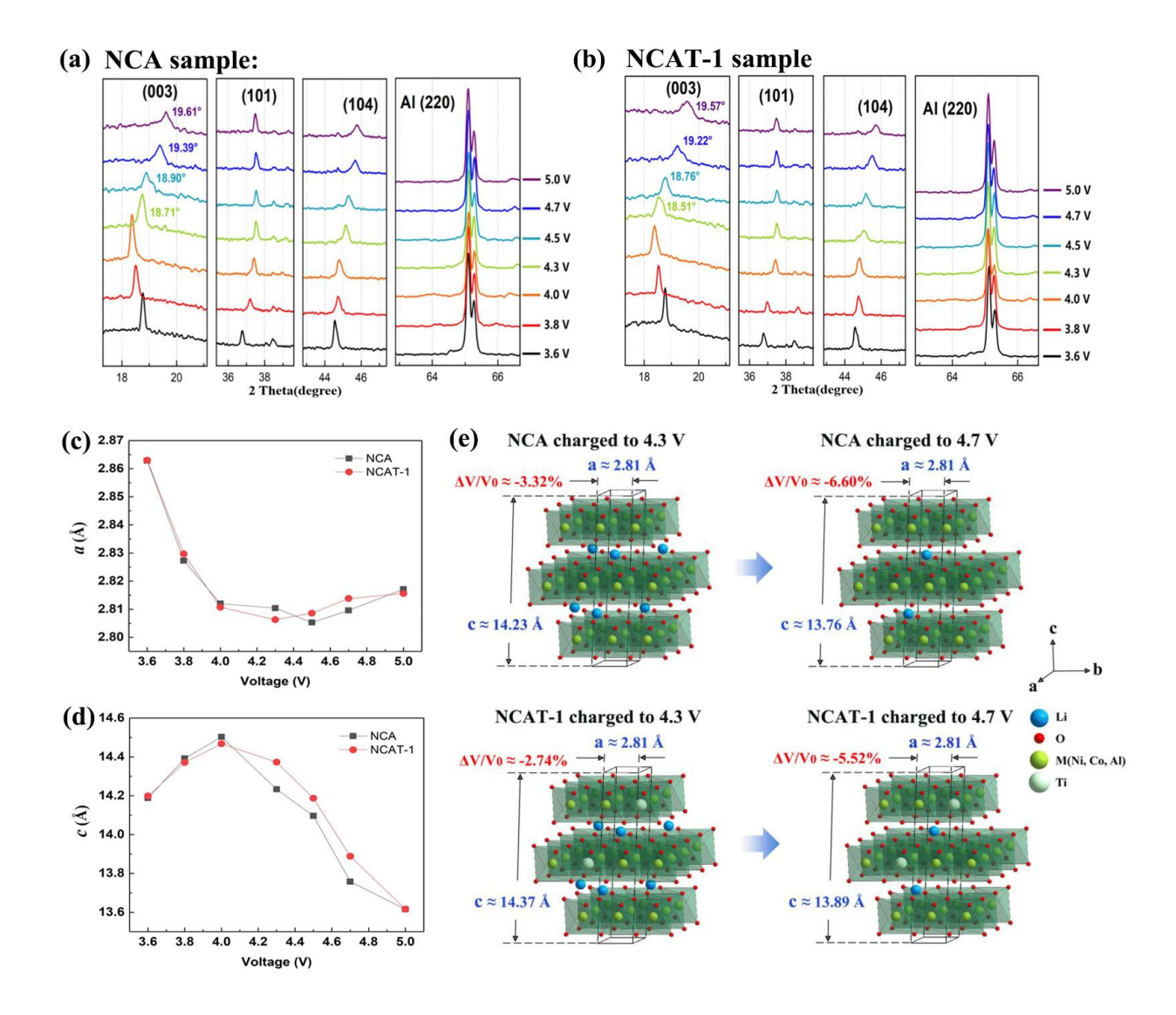


**Figure 5.** Ex-situ XRD patterns of (a) NCA and (b) NCAT-1 electrodes at different charge states from 3.6 V to 5.0 V. Curves of lattice parameters (c) *a* and (d) *c* vary with the charge states of NCA and NCAT-1 samples. (e) Lattice parameters and cell volumes evolution during charging process exhibited by 3D structural models.

two-theta angles and then move to higher angles, while the position of (101) and (104) diffraction peaks shows monotonic shifting to the higher angles with increased charge state. Since the (003)

plane is perpendicular to c-axis and sensitive to lattice parameter c, shifting of (003) peak to lower angles at the beginning of charging process indicates the expansion of c caused by the increased repulsion between adjacent oxygen atoms along the c-axis with the deintercalation of Li<sup>+</sup>. As the electrodes were further charged over 4.0 V, the (003) peak began to move to higher angles implying shrinkage along c direction caused by over deintercalation of Li<sup>+</sup>, leading to the distortion and even collapse of the layered structure. Additionally, the right shift of (101) and (104) peaks is a reflection of the shrinkage of the a- and b-axis along the charging process resulting from the reduced ion radii of transition metals at higher oxidation states. The lattice parameters and variation tendency with the charging process of the two samples derived from XRD patterns are plotted in Figure 5c and d. The evolution of parameter a is almost the same for both samples (Figure 5c), indicating Ti substitution in NCA does not significantly affect the changes of a-b plane during charge. In contrast, the shrinkage of parameter c at highly charged states is less severe for the Ti-substituted sample up to 4.7 V (Figure 5d), indicating that Ti ions in the lattice can stabilize the structure from collapsing along c axis effectively when the cell is charged to high voltage. For better understanding, Figure 5e illustrates the 3D structural models to demonstrate the geometry change of unit cell. The volume shrinkage of unit cell during the charging process, especially at high voltage states, is obviously decreased by Ti substitution, which is beneficial to reduce the lattice strain and suppress the formation of microcracks during cycling.

To study the impact of Ti-doping on charge compensation of NCA cathode during charge, XAS of the two samples at various charge states was performed. The Co and Ni K-edge XAS spectra for NCA and NCAT-1 are plotted in Figure S7. For Ni K-edge, the edge shift to higher energy can be clearly seen as the electrode is charged to 4.5 V, showing the oxidation of Ni in the charging process to 4.5 V. However, from 4.5 V to 4.7 V, Ni K-edge shows no shift, indicating that Ni does

not participate in charge compensation during charging above 4.5 V. For Co XAS spectra, the Co K-edge also shifts to higher energy, but much less than that of Ni K-edge, with edge shape changes. It suggests that Co also participate in charge compensation, but the contribution is less than Ni. In general, Ni and Co K-edge evolutions of NCA and NCAT-1 during charge are quite similar, implying Ti doping does not affect charge compensation of NCA from transition metals.

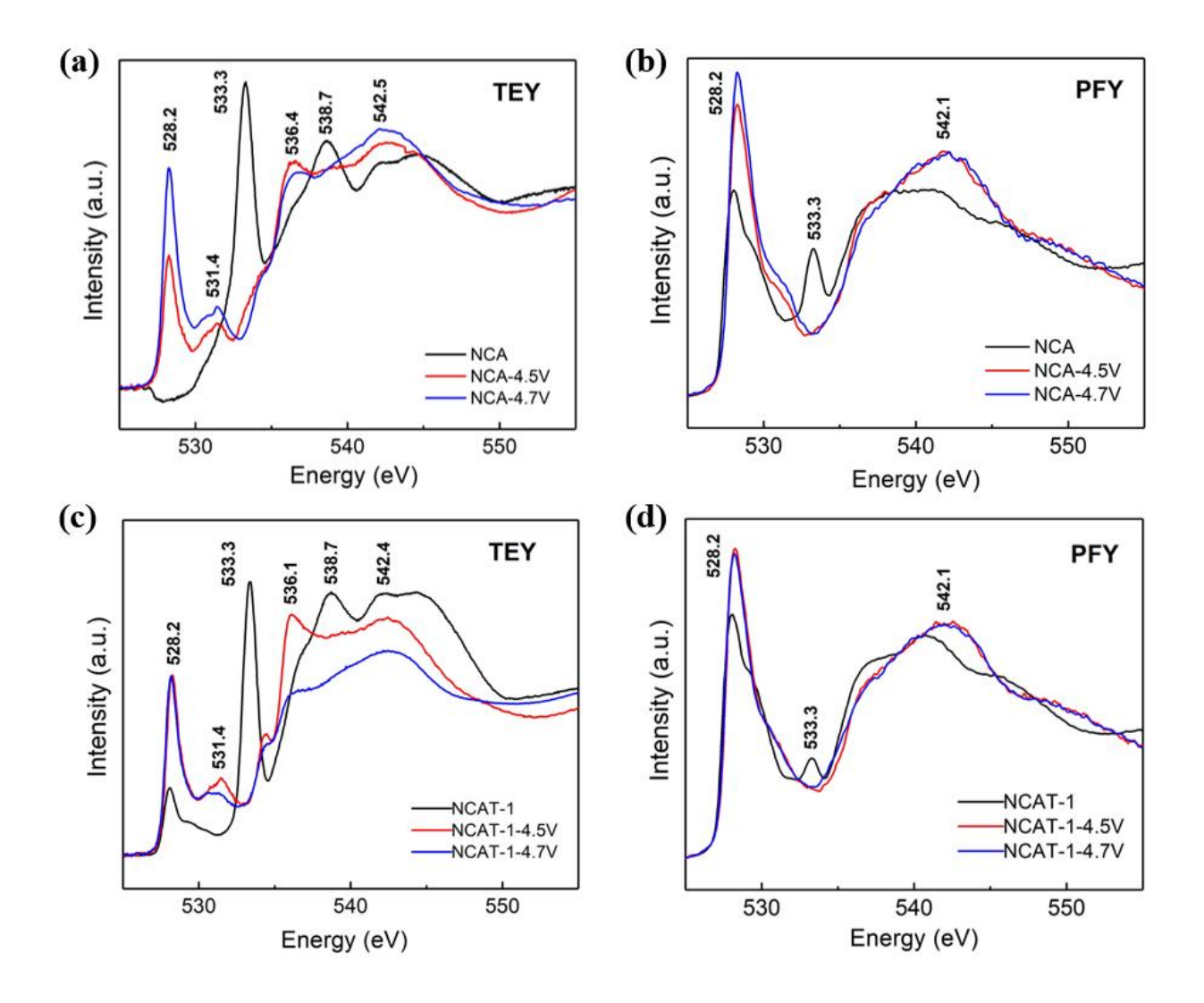


**Figure 6.** Soft XAS spectra of O K-edge for NCA in (a) TEY, (b) PFY modes and for NCAT-1 in (c) TEY, (d) PFY modes.

Since the evolution of oxygen ions in layer-structured cathode is highly related to their structural stability, especially during high voltage charging, the electronic structure of oxygen was studied by oxygen K-edge soft XAS. The O XAS spectra of NCA and NCAT-1 at different charge states in TEY and PFY modes are presented in Figure 6. It is known that TEY mode is surface sensitive (within ~5 nm), while the PFY probes the bulk with a depth of several hundred nm.<sup>39</sup> By doing both, a complementary information of the electronic structure for both surface and bulk can be gained. The sharp peak at 533.3 eV is ascribed to the transition of O 1s electron to the band mainly consisting of Ni-3d orbitals of rock-salt NiO.<sup>40</sup> In PFY mode, the peak at 533.3 eV decreases significantly at the initial state after Ti doping indicating a decrease in the amount of NiO, which agrees well with TEM results in Figure 2. The peaks at 528.2 and 531.4 eV are ascribed to the transition of O 1s electron to the hybridized state of transition metal 3d and O 2p orbitals, which splits into two peaks due to the different energies of the t<sub>2g</sub> and e<sub>g</sub> symmetries.<sup>41</sup> The broad peaks above 535 eV are assigned to O 1s electron excitations to hybridized states of O 2p and transitionmetal 4s and 4p orbitals. 42,43 The intensity of the peak at 528.2 eV increases obviously with the charge state elevated from 4.5 to 4.7 V both in TEY and PFY modes for NCA cathode. It means that the unoccupied density of states in the Ni3d-O2p bands increases due to the formation of O 2p electron holes with the further delithiation both at the surface and in the bulk. However, there is no significant change of the peak at 528.2 eV between the charge states of 4.5 and 4.7 V for NCAT-1 electrode. This suggests that Ti substitution suppresses the formation of O 2p holes as the charge state is elevated over 4.5 V, indicating less electronic structure changes of O in NCAT-1. Therefore, NCAT-1 can maintain better integrity of the crystal structure against the oxygen release and exhibit higher cycle stability during high voltage charge.

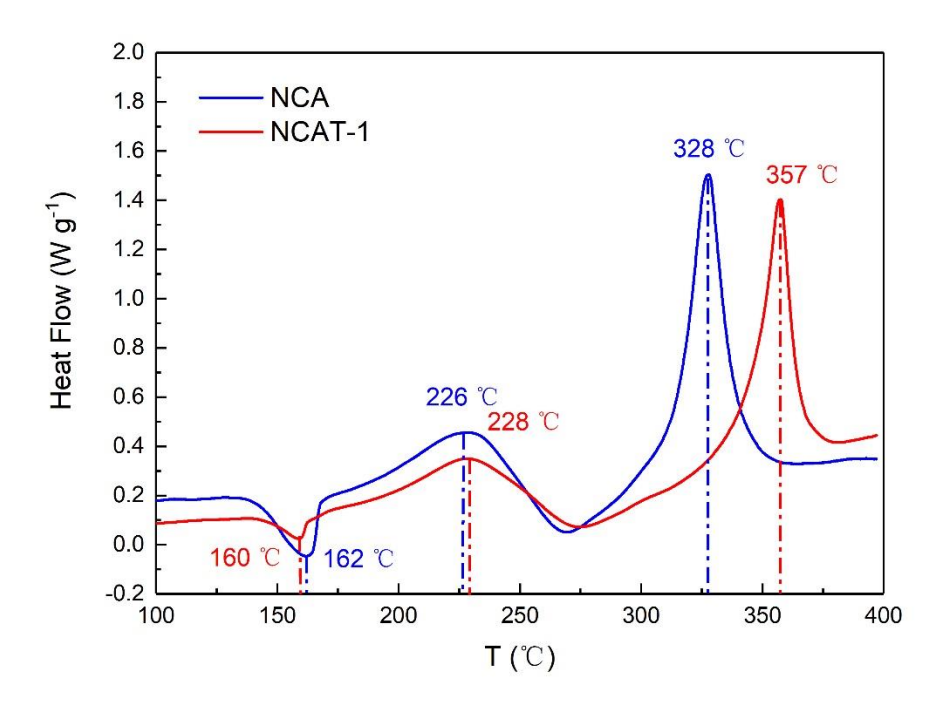


**Figure 7.** DSC curves of the NCA and NCAT-1 charged to 4.5 V.

**3.5. Thermal stability.** In practical application, thermal stability of electrode materials is another important factor that should be taken into special consideration in power sources for safety concern. <sup>44,45</sup> For the layer-structured cathode materials, the poor thermal stability of their crystal structure is always accompanied by oxygen release, <sup>46</sup> especially at the charged state, which is very harmful to the battery safety. For testing the thermal stability of NCA and NCAT-1, the two electrodes were charged to 4.5 V first, then the exothermic reactions were analyzed by DSC with the temperature slowly increased from 50 °C to 400 °C. As shown in Figure 7, two notable peaks at 226 °C and 328 °C for charged NCA can be observed, which are attributed to the two-step decomposition process from layered to spinel structure and from spinel to rock-salt structure, respectively. <sup>47</sup> For the NCAT-1 sample, the two peaks lie in 228 °C and 357 °C, higher than those

of NCA sample, with relatively lower peak intensities. It suggests that the decomposition of NCAT-1 takes place at a higher temperature and releases less heat, indicating better thermal stability than the pristine NCA. Combining with XRD and XAS results, the improvement of thermal stability can be attributed to the enhanced structural integrity and decreased O2p electron holes after Ti substitution.

#### 4. CONCLUSIONS

In this work, the effects of Ti substitution in NCA cathode on the electrochemical performance, structure evolution, charge compensation and thermal stability during high voltage charge are investigated systematically. The XRD and TEM results indicate that moderate Ti substitution in NCA cathode can effectively suppress the Li<sup>+</sup>/Ni<sup>2+</sup> mixing and the formation of NiO phase on surface. Under a high cut-off voltage of 4.7 V, NCAT-1 (1% Ti substitution) delivered the highest reversible capacity of 198.1 mA h g<sup>-1</sup> at 0.1 C with impressive capacity retention of 86.9% after 100 cycles. In addition, better kinetics property of NCAT-1 is also proved by its lower voltage polarization, higher Li<sup>+</sup> diffusion coefficient and rate capability, compared with NCA cathode. It is revealed that Ti substitution can successfully reduce the lattice distortion and stabilized the electronic structure of oxygen when charged to 4.7 V, which restrain the irreversible structure evolution and achieve enhanced cycle stability and thermal stability. This work provides in-depth understanding in element substitution, providing guidance for the utilization of high-voltage charging of layered cathodes for higher energy density. This is one step forward in the efforts to further increase the energy density of layer-structured cathode materials while minimizing negative impact on the cycle life and safety.

Table 1. Rietveld refinement results of XRD patterns of NCA, NCAT-0.5, NCAT-1 and NCAT-

2.

Sample	Lattice parameter		c/a	Cell volume	Li/Ni mixing	$\chi^2$	R <sub>p</sub> [%]	Rwp[%]
	a[Å]	c[Å]		$[Å^3]$	[%]			
NCA	2.8635(2)	14.1822(1)	4.9528	100.716	4.74	0.3691	1.63	2.32
NCAT-0.5	2.8646(1)	14.1916(4)	4.9541	100.854	1.56	0.7875	1.57	2.29
NCAT-1	2.8657(4)	14.1974(2)	4.9543	100.975	1.34	0.4049	1.53	2.09
NCAT-2	2.8677(1)	14.2141(2)	4.9566	101.232	1.82	0.5448	1.43	1.97

#### ASSOCIATED CONTENT

Electronic Supplementary Information (ESI) available: SEM images with EDS analysis; charge/discharge curves and coulombic efficiency; cycle stability between 3.0-4.3 V; Rietveld refinement result of XRD pattern, and K-edge XAS spectra of Co and Ni.

#### **AUTHOR INFORMATION**

#### **Corresponding Author**

\* E-mail: ynzhou@fudan.edu.cn; smbak@bnl.gov; xyang@bnl.gov

#### **Notes**

The authors declare no competing financial interest.

#### ACKNOWLEDGMENT

The work was financially supported by the NSFC (Grant No. 51502039 and 51671058). The work done at BNL was supported by Assistant Secretary for Energy Efficiency and Renewable Energy, Vehicle Technology Office of the U.S. DOE through the Advanced Battery Materials Research (BMR) Program, including Battery500 Consortium under contract DE-SC0012704. The authors thank beamlines 7-BM (QAS) and 23-ID-2 (IOS) of the NSLS II, a U.S. DOE Office of Science User Facility operated by BNL under Contract No. DE-SC0012704. The authors also thank beamline BL14W1 of SSRF.

#### **REFERENCES**

- 1. Li, M.; Lu, J.; Chen, Z. W.; Amine, K., 30 Years of Lithium-Ion Batteries. *Adv. Mater.* **2018,** *30*, 1800561.
- 2. Xu, J.; Lin, F.; Doeff, M. M.; Tong, W., A Review of Ni-based Layered Oxides for Rechargeable Li-ion Batteries. *J. Mater. Chem. A* **2017**, *5*, 874-901.
- 3. Armand, M.; Tarascon, J. M., Building Better Batteries. *Nature* **2008**, *451*, 652-657.

- 4. Nitta, N.; Wu, F. X.; Lee, J. T.; Yushin, G., Li-ion Battery Materials: Present and Future. *Mater. Today* **2015**, *18*, 252-264.
- 5. Wu, N. T.; Wu, H.; Yuan, W.; Liu, S. J.; Liao, J. Y.; Zhang, Y., Facile Synthesis of one-dimensional LiNi<sub>0.8</sub>Co<sub>0.15</sub>Al<sub>0.05</sub>O<sub>2</sub> Microrods as Advanced Cathode Materials for Lithium ion Batteries. *J. Mater. Chem. A* **2015**, *3*, 13648-13652.
- 6. Xie, H. B.; Du, K.; Hu, G. R.; Duan, J. G.; Peng, Z. D.; Zhang, Z. J.; Cao, Y. B., Synthesis of LiNi<sub>0.8</sub>Co<sub>0.15</sub>Al<sub>0.05</sub>O<sub>2</sub> with 5-sulfosalicylic Acid as a Chelating Agent and its Electrochemical Properties. *J. Mater. Chem. A* **2015**, *3*, 20236-20243.
- 7. Yang, X. R.; Chen, J. W.; Zheng, Q. F.; Tu, W. Q.; Xing, L. D.; Liao, Y. H.; Xu, M. Q.; Huang, Q. M.; Cao, G. Z.; Li, W. S., Mechanism of Cycling Degradation and Strategy to Stabilize a Nickel-rich Cathode. *J. Mater. Chem. A* **2018**, *6*, 16149-16163.
- 8. Yan, P. F.; Zheng, J. M.; Zhang, J. G.; Wang, C. M., Atomic Resolution Structural and Chemical Imaging Revealing the Sequential Migration of Ni, Co, and Mn upon the Battery Cycling of Layered Cathode. *Nano Lett.* **2017**, *17*, 3946-3951.
- 9. Jung, S. K.; Gwon, H.; Hong, J.; Park, K. Y.; Seo, D. H.; Kim, H.; Hyun, J.; Yang, W.; Kang, K., Understanding the Degradation Mechanisms of LiNi<sub>0.5</sub>Co<sub>0.2</sub>Mn<sub>0.3</sub>O2 Cathode Material in Lithium Ion Batteries. *Adv. Energy Mater.* **2014**, *4*, 1300787.
- 10. Lin, F.; Markus, I. M.; Nordlund, D.; Weng, T. C.; Asta, M. D.; Xin, H. L. L.; Doeff, M. M., Surface Reconstruction and Chemical Evolution of Stoichiometric Layered Cathode Materials for Lithium-ion Batteries. *Nat. Commun.* **2014**, *5*, 3529.
- 11. Watanabe, S.; Kinoshita, M.; Nakura, K., Capacity Fade of LiNi<sub>(1-x-y)</sub>Co<sub>x</sub>Al<sub>y</sub>O<sub>2</sub> Cathode for Lithium-ion Batteries during Accelerated Calendar and Cycle Life Test. I. Comparison Analysis between LiNi<sub>(1-x-y)</sub>Co<sub>x</sub>Al<sub>y</sub>O<sub>2</sub> and LiCoO<sub>2</sub> Cathodes in Cylindrical Lithium-ion Cells during Long Term Storage Test. *J. Power Sources* **2014**, *247*, 412-422.
- 12. Goodenough, J. B.; Kim, Y., Challenges for Rechargeable Li Batteries. *Chem. Mater.* **2010,** 22, 587-603.
- 13. Zheng, J. M.; Yan, P. F.; Zhang, J. D.; Engelhard, M.; Zhu, Z. H.; Polzin, B. J.; Trask, S.; Xiao, J.; Wang, C. M.; Zhang, J. G., Suppressed Oxygen Extraction and Degradation of LiNi<sub>x</sub>Mn <sub>v</sub>Co<sub>z</sub>O<sub>2</sub> Cathodes at High Charge Cut-off Voltages. *Nano Res.* **2017**, *10*, 4221-4231.
- 14. Kim, H.; Kim, M. G.; Jeong, H. Y.; Nam, H.; Cho, J., A New Coating Method for Alleviating Surface Degradation of LiNi $_{0.6}$ Co $_{0.2}$ Mn $_{0.2}$ O $_2$  Cathode Material: Nanoscale Surface Treatment of Primary Particles. *Nano Lett.* **2015**, *15*, 2111-2119.
- 15. Kiziltas-Yavuz, N.; Herklotz, M.; Hashem, A. M.; Abuzeid, H. M.; Schwarz, B.; Ehrenberg, H.; Mauger, A.; Julien, C. M., Synthesis, Structural, Magnetic and Electrochemical Properties of LiNi<sub>1/3</sub>Mn<sub>1/3</sub>Co<sub>1/3</sub>O<sub>2</sub> Prepared by a Sol-Gel Method using Table Sugar as Chelating Agent. *Electrochim. Acta* **2013**, *113*, 313-321.
- 16. Yan, P. F.; Zheng, J. M.; Gu, M.; Xiao, J.; Zhang, J. G.; Wang, C. M., Intragranular Cracking as a Critical Barrier for High-Voltage Usage of Layer-Structured Cathode for Lithiumion Batteries. *Nat. Commun.* **2017**, *8*,14101.
- 17. Du, K.; Xie, H. B.; Hu, G. R.; Peng, Z. D.; Cao, Y. B.; Yu, F., Enhancing the Thermal and Upper Voltage Performance of Ni-Rich Cathode Material by a Homogeneous and Facile Coating Method: Spray-Drying Coating with Nano-Al<sub>2</sub>O<sub>3</sub>. *ACS Appl. Mater. Interfaces* **2016**, *8*, 17713-17720.
- 18. Lai, Y. Q.; Xu, M.; Zhang, Z. A.; Gao, C. H.; Wang, P.; Yu, Z. Y., Optimized Structure Stability and Electrochemical Performance of LiNi<sub>0.8</sub>Co<sub>0.15</sub>Al<sub>0.05</sub>O<sub>2</sub> by Sputtering Nanoscale ZnO Film. *J. Power Sources* **2016**, *309*, 20-26.

- 19. Yan, X. X.; Chen, L.; Shah, S. A.; Liang, J. J.; Liu, Z. F., The Effect of Co<sub>3</sub>O<sub>4</sub> & LiCoO<sub>2</sub> Cladding Layer on the High Rate and Storage Property of High Nickel Material LiNi<sub>0.8</sub>Co<sub>0.15</sub>Al<sub>0.05</sub>O<sub>2</sub> by Simple One-Step Wet Coating Method. *Electrochim. Acta* **2017**, *249*, 179-188.
- 20. He, X. S.; Du, C. Y.; Shen, B.; Chen, C.; Xu, X.; Wang, Y. J.; Zuo, P. J.; Ma, Y. L.; Cheng, X. Q.; Yin, G. P., Electronically Conductive Sb-doped SnO<sub>2</sub> Nanoparticles Coated LiNi<sub>0.8</sub>Co<sub>0.15</sub>Al<sub>0.05</sub>O<sub>2</sub> Cathode Material with Enhanced Electrochemical Properties for Li-ion Batteries. *Electrochim. Acta* **2017**, *236*, 273-279.
- 21. Wu, N. T.; Wu, H.; Liu, H.; Zhang, Y., Solvothermal Coating LiNi<sub>0.8</sub>Co<sub>0.15</sub>Al<sub>0.05</sub>O<sub>2</sub> Microspheres with Nanoscale Li<sub>2</sub>TiO<sub>3</sub> Shell for Long Lifespan Li-ion Battery Cathode Materials. *J. Alloy. Compd.* **2016**, *665*, 48-56.
- 22. Zhang, X. D.; Shi, J. L.; Liang, J. Y.; Yin, Y. X.; Zhang, J. N.; Yu, X. Q.; Guo, Y. G., Suppressing Surface Lattice Oxygen Release of Li-Rich Cathode Materials via Heterostructured Spinel Li<sub>4</sub>Mn<sub>5</sub>O<sub>12</sub> Coating. *Adv. Mater.* **2018**, *30*, 1801751.
- 23. Markus, I. M.; Lin, F.; Kam, K. C.; Asta, M.; Doeff, M. M., Computational and Experimental Investigation of Ti Substitution in Li<sub>1</sub>(Ni<sub>x</sub>Mn<sub>x</sub>Co<sub>1-2x-y</sub>Ti<sub>y</sub>)O<sub>2</sub> for Lithium Ion Batteries. *J. Phys. Chem. Lett.* **2014**, *5*, 3649-3655.
- 24. Du, R.; Bi, Y. J.; Yang, W. C.; Peng, Z.; Liu, M.; Liu, Y.; Wu, B. M.; Yang, B. C.; Ding, F.; Wang, D. Y., Improved Cyclic Stability of LiNi<sub>0.8</sub>Co<sub>0.1</sub>Mn<sub>0.1</sub>O<sub>2</sub> via Ti Substitution with a Cutoff Potential of 4.5 V. *Ceram. Int.* **2015**, *41*, 7133-7139.
- 25. Nurpeissova, A.; Choi, M. H.; Kim, J. S.; Myung, S. T.; Kim, S. S.; Sun, Y. K., Effect of Titanium Addition as Nickel Oxide Formation Inhibitor in Nickel-Rich Cathode Material for Lithium-ion Batteries. *J. Power Sources* **2015**, *299*, 425-433.
- 26. Huang, B.; Li, X. H.; Wang, Z. X.; Guo, H. J.; Xiong, X. H., Synthesis of Mg-doped LiNi<sub>0.8</sub>Co<sub>0.15</sub>Al<sub>0.05</sub>O<sub>2</sub> Oxide and its Electrochemical Behavior in High-Voltage Lithium-ion Batteries. *Ceram. Int.* **2014**, *40*, 13223-13230.
- 27. Schipper, F.; Dixit, M.; Kovacheva, D.; Talianker, M.; Haik, O.; Grinblat, J.; Erickson, E. M.; Ghanty, C.; Major, D. T.; Markovsky, B.; Aurbach, D., Stabilizing Nickel-rich Layered Cathode Materials by a High-Charge Cation Doping Strategy: Zirconium-Doped LiNi<sub>0.6</sub>Co<sub>0.2</sub>Mn<sub>0.2</sub>O<sub>2</sub>. *J. Mater. Chem. A* **2016**, *4*, 16073-16084.
- 28. Qi, Y. L.; Huang, Y. D.; Jia, D. Z.; Bao, S. J.; Guo, Z. P., Preparation and Characterization of Novel Spinel Li<sub>4</sub>Ti<sub>5</sub>O<sub>12-x</sub>Br<sub>x</sub> Anode Materials. *Electrochim. Acta* **2009**, *54*, 4772-4776.
- 29. Li, X.; Xie, Z. W.; Liu, W. J.; Ge, W. J.; Wang, H.; Qu, M. Z., Effects of Fluorine Doping on Structure, Surface Chemistry, and Electrochemical Performance of LiNi<sub>0.8</sub>Co<sub>0.15</sub>A1<sub>0.05</sub>O<sub>2</sub>. *Electrochim. Acta* **2015**, *174*, 1122-1130.
- 30. Yue, J. L.; Zhou, Y. N.; Yu, X. Q.; Bak, S. M.; Yang, X. Q.; Fu, Z. W., O3-type Layered Transition Metal Oxide Na(NiCoFeTi)<sub>1/4</sub>O<sub>2</sub> as a High Rate and Long Cycle Life Cathode Material for Sodium ion Batteries. *J. Mater. Chem. A* **2015**, *3*, 23261-23267.
- 31. Zhou, Y. N.; Ma, J.; Hu, E. Y.; Yu, X. Q.; Gu, L.; Nam, K. W.; Chen, L. Q.; Wang, Z. X.; Yang, X. Q., Tuning Charge-Discharge Induced Unit Cell Breathing in Layer-Structured Cathode Materials for Lithium-ion Batteries. *Nat. Commun.* **2014**, *5*, 5381.
- 32. Zhou, Y. N.; Yue, J. L.; Hu, E.; Li, H.; Gu, L.; Nam, K. W.; Bak, S. M.; Yu, X.; Liu, J.; Bai, J.; Dooryhee, E.; Fu, Z. W.; Yang, X. Q., High-Rate Charging Induced Intermediate Phases and Structural Changes of Layer-Structured Cathode for Lithium-Ion Batteries. *Adv. Energy Mater.* **2016**, *6*, 160597.

- 33. Wang, Y.-Y.; Sun, Y.-Y.; Liu, S.; Li, G.-R.; Gao, X.-P., Na-Doped LiNi<sub>0.8</sub>Co<sub>0.15</sub>Al<sub>0.05</sub>O<sub>2</sub> with Excellent Stability of Both Capacity and Potential as Cathode Materials for Li-Ion Batteries. *ACS Applied Energy Materials* **2018**, *1*, 3881-3889.
- 34. Myung, S. T.; Maglia, F.; Park, K. J.; Yoon, C. S.; Lamp, P.; Kim, S. J.; Sun, Y. K., Nickel-Rich Layered Cathode Materials for Automotive Lithium-Ion Batteries: Achievements and Perspectives. *ACS Energy Lett.* **2017**, *2*, 196-223.
- 35. Myung, S. T.; Izumi, K.; Komaba, S.; Sun, Y. K.; Yashiro, H.; Kumagai, N., Role of Alumina Coating on Li-Ni-Co-Mn-O Particles as Positive Electrode Material for Lithium-ion Batteries. *Chem. Mater.* **2005**, *17*, 3695-3704.
- 36. Kam, K. C.; Mehta, A.; Heron, J. T.; Doeff, M. M., Electrochemical and Physical Properties of Ti-Substituted Layered Nickel Manganese Cobalt Oxide (NMC) Cathode Materials. *J. Electrochem. Soc.* **2012**, *159*, A1383-A1392.
- 37. Wang, Q. C.; Qiu, Q. Q.; Xiao, N.; Fu, Z. W.; Wu, X. J.; Yang, X. Q., Zhou, Y. N., Tunnel-Structured  $Na_{0.66}[Mn_{0.66}Ti_{0.34}]O_{2-x}F_x$  (x < 0.1) Cathode for High Performance Sodium-ion Batteries. *Energy Storage Mater.* **2018**, *15*, 1-7.
- 38. Robert, R.; Bunzli, C.; Berg, E. J.; Novak, P., Activation Mechanism of LiNi<sub>0.80</sub>Co<sub>0.15</sub>Al<sub>0.05</sub>O<sub>2</sub>: Surface and Bulk Operando Electrochemical, Differential Electrochemical Mass Spectrometry, and X-ray Diffraction Analyses. *Chem. Mater.* **2015**, *27*, 526-536.
- 39. Yoon, W. S.; Balasubramanian, M.; Chung, K. Y.; Yang, X. Q.; McBreen, J.; Grey, C. P.; Fischer, D. A., Investigation of the Charge Compensation Mechanism on the Electrochemically Li-ion Deintercalated Li<sub>1-x</sub>Co<sub>1/3</sub>Ni<sub>1/3</sub>Mn<sub>1/3</sub>O<sub>2</sub> Electrode System by Combination of Soft and Hard X-ray Absorption Spectroscopy. *J. Am. Chem. Soc.* **2005**, *127*, 17479-17487.
- 40. Palina, N.; Wang, L.; Dash, S.; Yu, X. J.; Breese, M. B. H.; Wang, J. L.; Rusydi, A., Investigation of the Metal-Insulator Transition in NdNiO<sub>3</sub> Films by Site-Selective X-ray Absorption Spectroscopy. *Nanoscale* **2017**, *9*, 6094-6102.
- 41. Ma, J.; Zhou, Y. N.; Gao, Y. R.; Kong, Q. Y.; Wang, Z. X.; Yang, X. Q.; Chen, L. Q., Molybdenum Substitution for Improving the Charge Compensation and Activity of Li<sub>2</sub>MnO<sub>3</sub>. *Chem-Eur. J.* **2014**, *20*, 8723-8730.
- 42. Yoon, W. S.; Chung, K. Y.; McBreen, J.; Fischer, D. A.; Yang, X. Q., Electronic Structural Changes of the Electrochemically Li-ion Deintercalated LiNi<sub>0.8</sub>Co<sub>0.15</sub>Al<sub>0.05</sub>O<sub>2</sub> Cathode Material Investigated by X-ray Absorption Spectroscopy. *J. Power Sources* **2007**, *174*, 1015-1020.
- 43. Wang, Q. C.; Meng, J. K.; Yue, X. Y.; Qiu, Q. Q.; Song, Y.; Wu, X. J.; Fu, Z. W.; Xia, Y. Y.; Shadike, Z.; Wu, J.; Yang, X. Q.; Zhou, Y. N., Tuning P2-Structured Cathode Material by Na-Site Mg Substitution for Na-Ion Batteries. *J. Am. Chem. Soc.* **2019**, *141*, 840-848.
- 44. Hou, P.; Yin, J.; Ding, M.; Huang, J.; Xu, X., Surface/Interfacial Structure and Chemistry of High-Energy Nickel-Rich Layered Oxide Cathodes: Advances and Perspectives. *Small* **2017**, *13*, 1701802.
- 45. Wu, L.; Nam, K.-W.; Wang, X.; Zhou, Y.; Zheng, J.-C; Yang, X.-Q; Zhu, Y., Structural Origin of Overcharge-Induced Thermal Instability of Ni-Containing Layered-Cathodes for High-Energy-Density Lithium Batteries. *Chem. Mater.* **2011**, *23*, 3953-3960.
- 46. Bak, S. M.; Hu, E.; Zhou, Y.; Yu, X.; Senanayake, S. D.; Cho, S. J.; Kim, K. B.; Chung, K. Y.; Yang, X. Q.; Nam, K. W. Structural Changes and Thermal Stability of Charged LiNi<sub>x</sub>Mn<sub>y</sub>Co<sub>z</sub>O<sub>2</sub> Cathode Materials Studied by Combined In Situ Time-Resolved XRD and Mass Spectroscopy. *ACS Appl. Mater. Interfaces.* **2014**, *6*, 22594-22601.
- 47. Nam, K.-W.; Bak, S.-M.; Hu, E.; Yu, X.; Zhou, Y.; Wang, X.; Wu, L.; Zhu, Y.; Chung, K.-Y.; Yang, X.-Q., Combining In Situ Synchrotron X-Ray Diffraction and Absorption

Techniques with Transmission Electron Microscopy to Study the Origin of Thermal Instability in Overcharged Cathode Materials for Lithium-Ion Batteries. *Adv. Funct. Mater.* **2013**, *23*, 1047-1063.

## TOC figure

